*Chapter 3*

# IMAGING NEUROPEPTIDE LOCALIZATION AND RELEASE IN MAMMALIAN CELLS WITH NOVEL GENETICALLY ENGINEERED REPORTERS

**Summary**

Neuropeptides are essential to the regulation of a variety of developmental, physiological, and behavioral functions. However, the subcellular localization and release properties of neuropeptides are less understood. Here we report the development of two sets of genetically engineered reporters: Neuropeptide Localization and Expression reporters (NPLER) and Neuropeptide Release Reporters (NPRR) and their applications in N46, a novel peptidergic cell line. The investigation of two neuropeptides of interest, NPY and NkB reveals previously unexplored differences in the sorting, routing, and release processes. Furthermore, we transformed PC12 cells with NPLER to generate a prototypical generic platform that potentially accelerates large-scale RNAi screening.

## Introduction

Neuropeptides play significant roles in modulating neuronal activities (Hökfelt et al., 2003; Nusbaum et al., 2017; van den Pol, 2012). In mammals, over 100 neuropeptides are discovered and studied (Russo, 2017; van den Pol, 2012). It is generally accepted that (1) each neuropeptide owns its unique expression pattern throughout the brain and some peripheral endocrine cells; (2) each neuropeptide has distinct functions; (3) each peptidergic neuron/cell usually contains more than one type of neuropeptide. However, these studies offered limited insight as (1) mainly focused on cell lines originated from peripheral tissues, such as pancreas and adrenal glands; (2) only very few neuropeptides were studied. Many fluorescent protein-fused neuropeptide reporters were generated,

but they functioned mostly as proxies for secretory granule properties. There is a huge gap between the current strategies to develop novel tools or platforms, and the ambition of demystifying the complexity of neuropeptides. In this study, we established a prototypic platform that contains an adequate cell line and two sets of genetically engineered reporters: Neuropeptide Localization and Expression Reporters (NPLERs) and Neuropeptide Release Reporters (NPRRs). Two neuropeptides of interest, Neurokinin B (NkB) and Neuropeptide Y (NPY), were studied in this platform. We provided lines of evidence that NkB and NPY have distinct localization and routing destinations, and their subdomains function differently. NPRR studies prove that physiologically relevant stimuli, such as PACAP, triggers NPY release. Lastly, we tested the potential of transforming a canonical cell line to a generalized platform for studies of exogenous neuropeptides and regulations.

## Results

### A novel cell line for neuropeptide imaging

We selected two neuropeptides of interest for this study: Neurokinin B (NkB) and Neuropeptide Y (NPY), for their well-characterized physiological functions and strong clinical significance. NPY plays an essential role in feeding (Hökfelt et al., 2008; Luquet et al., 2005), energy balance (Loh et al., 2015) and stress (Heilig, 2004; Hirsch & Zukowska, 2012). NPY receptor antagonists were heavily invested to battle obesity and diabetes (Williams et al., 2020; Yulyaningsih et al., 2011), but none has survived to the New Drug Application (NDA) phase. NkB (Tac2) was mostly associated with ovulatory cycles (Hall, 2019) and airway diseases (Piedimonte, 1995). NK3R antagonists are but recent studies uncovered NkB functions in the central brain, such as coordination of a pleiotropic brain state caused by chronic social isolation (Zelikowsky et al., 2018).

We therefore sought to find cell lines that endogenously express NkB and/or NPY. Hypothalamic cells are known for enriched expression of neuropeptides (Parker & Bloom, 2012). Previous efforts of immortalizing hypothalamic cells result in a wide collection of neuropeptidergic cell lines (Belsham et al., 2004). Each cell line has a unique neuropeptide expression profile, characterized at the mRNA level by RT-PCR (Belsham et al., 2004). We resorted to the profiles and shortlisted 5 hypothalamic cell lines based on their expression of NkB or NPY, including 2 embryonic cell lines (mHypoE-N7, mHypoE-N46) and 3 adult cell lines (mHypoA-2/29, mHypoA-2/32, mHypoA-59) (Figure 1A). MIN-6β, an insulinoma cell line, was also included because of its popular use in the investigation of secretory granule release (Figure 1A) (Rutter et al., 2006; Varadi et al., 2005). We employed immunocytochemistry with NkB and NPY antibodies for further validations, the results were generally consistent with RT-PCR (Figure 1B). We next asked if these cell lines sort and transport neuropeptides properly. We modified NPY-GFP, a canonical secretory granule marker, by replacing its human NPY fragment with mouse NPY, all else unaltered. To distinguish the new reporter from NPY-GFP, we named it NPLER$^{NPYfl\text{-}GFP}$ (details discussed later) (Figure 1C). Transfection of this new reporter gave rise to fluorescence in all cell lines, but only the embryonic cell lines (mHypoE-N7 and mHypoE-N46) showed nicely colocalized double-labelings of GFP and NPY (Figure 1D$_1$). In mHypoE-N7 cells, the majority of fluorescence resides in the peri-nucleus region, likely ER and golgi apparatus. Little fluorescence was seen in the processes. mHypoE-N46 cells, on the contrary, possessed dispersed fluorescent puncta throughout the cell, strongly indicative of appropriate sorting and trafficking of the NPLER transgene. Parallel experiment of mHypoE-N46 cells without NPLER$^{NPYfl\text{-}GFP}$ suggested that the green fluorescence was not contributed by cell autofluorescence (Figure 1D$_2$). Therefore, mHypoE-N46 cells (N46 cells in the following context)

were chosen as the NPY reporter testbed. Moreover, N46 cell line was the only candidate that endogenously expresses both NPY and NkB, supported by both RT-PCR data and immunocytochemistry (Figure 1A-B). It is likely that N46 cells also makes ways for NkB reporter screenings.

We then asked if N46 cells can release neuropeptides. High potassium challenge triggers neuropeptide release in fruit flies (Bulgari et al., 2018; Ding et al., 2019), neuroblastoma cell line (Ou et al., 1998) and hypothalamic explant (Dube et al., 1992; Gamber et al., 2005). High potassium stimulation triggers intense depolarization and massive neuropeptide release (Cavadas et al., 2002; Wang et al., 2016), resulting in the decrease of intracellular neuropeptide load (Figure 1B). We therefore designed a KCl stimulation experiment in which two parallel groups of cells were incubated in control buffer and high potassium buffer, respectively (Figure 2C). The cells were stained against NPY or NkB subsequently. NPY staining in control cells have significantly higher fluorescent intensity (****P<0.0001, Mann Whitney *U* test) (Figure 2D). NkB staining showed similar results, yet the difference between control and KCl challenged group was smaller (*P<0.05, Mann Whitney *U* test). The decrease of intracellular fluorescence reflects the release of primed neuropeptides to the extracellular spaces. We conclude that N46 cells are capable of releasing NkB and NPY.

**Design, screening, and validation of NPLERs**

We previously described the development and application of Neuropeptide Release Reporters (NPRRs) (Ding et al., 2019; Han & Ding, 2022) in *drosophila*. A genetically encoded NPRR should contain at least (1) a reporter domain that reflects the physico-chemical contrast between the

intravesicular milieu and the extracellular space and (2) a sorting domain that ensures its selective trafficking into DCVs (Figure $3A_1$). We reasoned that the configuration of *Drosophila* NPRR is applicable to mammals, as neuropeptides and their processing enzymes are highly evolutionarily conserved (Hoyle, 1998).

In parallel, we propose a set of sister reporters to visualize the intracellular expression and localization of neuropeptides. These new Neuropeptide Localization and Expression Reporters (NPLERs) were designed to share the same sorting domain with NPRRs (Figure $3A_2$), but do not experience fluorescent rise upon DCV fusion (Figure 3B). An appropriate NPLER reporter domain should have high brightness, high photostability and pH-invariant fluorescence. Therefore, the pKa of NPLER reporter domain falls between 3 and 5.5. NPRRs, on the contrary, entail reporter domains of higher pKa (5.5-7.4) to capitalize on the pH sensitivity (Figure 3C). We identified 8 NPLER reporter domain candidates and ~10 NPRR reporter domain candidates, based on the brightness/pKa profiles and cell line expression screening. Many widely used exocytosis markers and vesicle fusion reporters contain enhanced GFP (eGFP) fragments, we included them as reference NPLER reporter domains (Figure 3D), even though its pKa is higher than 5.5 (eGFP:~6.0). Other candidates include three GFP mutants (mTurqoise2 (mTq2), Gamillus, mVenus), mCherry and mKO2. NPRR reporter domain candidates are comprised of some latest pH-sensitive sensors, such as pHmScarlet variants (Liu et al., 2021) and novel pHluorins (unpublished data), and some genetically engineered calcium indicators (GECIs), such as GCaMP6s (Chen et al., 2013), low calcium affinity GCaMP6 derivatives(de Juan-Sanz et al., 2017) and B-GECO-1 (Zhao et al., 2011) (Figure 3D).

NPY prepropeptide contains 3 domains, a 28-aa signal peptide at N terminus, NPY domain, and a CPON domain (C peptide of NPY). It was proposed that the signal peptide of NPY is sufficient for DCV sorting process (El Meskini et al., 2001), we therefore renamed it signal/sorting peptide to highlight its potential dual functions (Figure $3E_1$). NkB signal peptide was too renamed in this study to avoid confusion, although its role in DCV sorting remains unclear (Figure $3E_2$). We designed three versions of NPY sorting domains, including the full length ($NPY_{fl}$), the CPON-depleted fragment that truncates at the $64^{th}$ amino acid ($NPY_{64}$) and 28-aa signal/sorting peptide only fragment ($NPY_{28}$) (Figure $3E_1$). All reporter domains were concatenated at the C-terminus of sorting domains, an empirical practice from the *Drosophila* NPRR screening to ensure strong fluorescent brightness of reporters (Ding et al., 2019). The combinations of both domain candidates, together with variation of linker sequence in some cases, result in a pool of ~30 $NPLER^{NPY}$ candidates. mTurqoise2 and mVenus and mCherry outperform others as best reporter domains. NkB sorting domains were designed with similar strategies, though NkB prepropeptide encompasses four domains. We assumed that the best reporter candidates from $NPLER^{NPY}$ screening function equally well for NkB, and generated 12 $NPLER^{NkB}$ candidates with all possible combinations (Figure $3E_2$).

We next asked if the various compositions of sorting domains lead to differences in localization and expression of reporters. We compared four reporters: $NPLER^{NPYfl\text{-}GFP}$, $NPLER^{NPYfl\text{-}mTq2}$, $NPLER^{NPY64\text{-}mTq2}$ and $NPLER^{NPY28\text{-}mTq2}$ via antibody staining against mTq2 or GFP (Figure $4A_1$). Expression of reporters was observed in all groups, as compared with the non-transfected control (Figure $4A_2$). We then compared two reporters without full-length NPY prepropeptide as their sorting domains. N46 cells transfected with either $NPLER^{NPY28\text{-}mTq2}$ (CMV-$NPY_{28}$-mTq2) (Figure $4B_1$) or $NPLER^{NPY64\text{-}mTq2}$ (CMV-$NPY_{64}$-mTq2) (Figure $4B_2$) showed perfect colocalization of NPY

staining and GFP staining (Figure 4B). It was not surprising in the case of NPLER$^{NPY64\text{-}mTq2}$, as the sorting domain contains the entire NPY peptide reactive to the antibody. Nevertheless, NPLER$^{NPY28\text{-}mTq2}$ does not contain NPY fragment in its design. NPY staining signals were solely contributed by endogenous NPY. Colocalization of endogenous NPY and NPLER$^{NPY28\text{-}mTq2}$ suggest that the 28-aa signal peptide of NPY is sufficient to drive the proper sorting and trafficking of a reporter domain in N46 cells. The sorting/trafficking function of NPY signal peptide in the hypothalamic cell line is consistent with the reports in corticotrope tumor cells and PC12 cells (El Meskini et al., 2001).

In all reporters with sorting domain variations, we noticed that some cells showed a perinucleus fluorescent patch (indicated by red triangle, Figure 4A$_1$), while some do not (white triangle, Figure 4A$_1$). The former may suggest accumulation of immature NPLER molecules in ER or Golgi apparatus. We counted the ratio of cells showing such accumulation over all transfected cells. Around 50-65% of cells showed such "perinucleus cap" (NPLER$^{NPYfl\text{-}GFP}$: 20/38, 52.6%; NPLERNPY$^{64\text{-}mTq2}$: 27/44, 61.4%; NPLER$^{NPY28\text{-}mTq2}$: 23/55, 51.1%). The accumulation may result from the overexpression of CMV-driven NPLER in some cells. We further compared the subcellular distribution of these two NPLER$^{NPY}$ candidates with organelle-specific markers that label ER or Golgi apparatus (ER: Calreticulin, TGN: TGN-38) (Figure 4C-D). The strong NPLER fluorescence hindered us from accurate quantification of overlap (Manders Coefficients), we turned to the processes of the cells. A small fraction of NPLER signals overlap with either ER or Golgi marker in the processes, and no statistically significant difference was found between NPLER$^{NPY64\text{-}mTq2}$ and NPLER$^{NPY28\text{-}mTq2}$ (Figure 4C$_3$, D$_3$).

To further compare the subcellular trafficking and distribution of NPLER$^{NPY}$ candidates, reporters with different length of sorting domains were paired in all possible combinations and co-transfected

in N46 cells (Figure 5). Direct comparisons between $NPY_{fl}$ vs. $NPY_{64}$ (Figure 5A), $NPY_{fl}$ vs. $NPY_{28}$ (Figure 5B) and $NPY_{64}$ vs. $NPY_{28}$ (Figure 5C) all showed highly colocalized distribution in the processes, while the extent of retention near the perinucleus region differ. We conclude that all tested sorting domains of NPY, including the signal/sorting peptide only version, can route NPLERs in an efficient fashion, as how neuropeptides are processed.

We subsequently tested mTq2-based $NPLER^{NkB}$ candidates that vary in sorting domains (Figure 6A). Native fluorescence of two longer versions, $NPLER^{NkBfl\text{-}mTq2}$ ($NPLER^{NkB\text{-}1}$) and $NPLER^{NkB91\text{-}mTq2}$ ($NPLER^{NkB\text{-}2}$), exhibited fluorescent puncta in the processes, while the two shorter ones did not. Instead, the mesh-shaped pattern in $NPLER^{NkB79\text{-}mTq2}$ ($NPLER^{NkB\text{-}3}$) highly suggested ER retention. The signal peptide only $NPLER^{NkB\text{-}4}$ barely presented signals (Figure 6B). The distribution of $NPLER^{NkB\text{-}3}$ led to the hypothesis that the C-terminus domains of NkB proprepeptide are involved in proper sorting and trafficking downstream of ER processing. Therefore, we investigated the cellular organelle distribution of two best candidates $NPLER^{NkB\text{-}1}$ and $NPLER^{NkB\text{-}2}$ via organelle-specific marker labeling (ER: Calreticulin, TGN: TGN-38) (Figure 6C). Quantification with Manders Overlap Coefficient (MOC) showed no significant difference between two candidates in the Golgi apparatus (Figure $6C_2$), yet a much higher fraction of $NPLER^{NkB\text{-}2}$ was found in ER, suggesting that $NPLER^{NkB\text{-}1}$ release from ER to the downstream more efficiently (Figure $6C_1$). Taken together, we believe that the full-length sorting domain is required for an optimal $NPLER^{NkB}$.

**NPLER reveals distinct routing properties of NkB and NPY**

The NPLER functions as a proxy for neuropeptide localization, which allowed us to ask how NPY and NkB distribute in a cell. Double labeling of neuropeptides is challenging, as most efficient

neuropeptide antibodies are generated from rabbits. In the case of NPY, staining with antibodies of mouse or goat origins fail to show puncta pattern. We co-transfected two NPLERs, NPLER$^{NPYfl\text{-}mCherry}$ and NPLER$^{NkBfl\text{-}mTq2}$ (Figure 7A) in N46 cells. Surprisingly, they did not colocalize, particularly in the processes of the cells (Figure 7B). To test if the pattern results from the peculiarity of N46 cells, we performed a parallel experiment with the rat pheochromocytoma PC12 cells, a canonical cell line for studying neuromodulation, via co-transfection of the same reporters (Figure 7A). The NPLER$^{NPY}$ puncta were distinct from the NPLER$^{NkB}$ puncta (Figure 7C). Moreover, the relative scarcity of the latter reporter coincided with the expression profile of PC12 cells, which express high level of NPY but no NkB (Figure 7D).

Unlike small-molecule neurotransmitters, neuropeptides are routed into dense core vesicles for release (van den Pol, 2012). DCVs were identified via electron microscopy and named for the enhanced electron density in the vesicle lumen (De Camilli & Jahn, 1990). They also bear heterogeneity in sizes and molecular machineries, resulting in a panel of many DCV markers, notably members of the chromogranin and secretogranin families (De Camilli & Jahn, 1990; Huttner et al., 1991; Taupenot et al., 2003). These markers were mostly found in chromaffin cells, but were later found commonly shared by other cell types (Montero-Hadjadje et al., 2007; Winkler & Fischer-Colbrie, 1992). The availability of antibodies targeting some of them, in this case Chromogranin A (ChgA), Chromogranin B (ChgB), Secretogranin II (ScgII), Secretogranin III (ScgIII) and Secretogranin V (ScgV), allowed us to ask if NPY and NkB enter DCVs, and if so, of what kind. We tried to test the expression of DCV markers via antibody staining in N46 cells, but observed inconclusive fluorescent pattern caused by high background. Therefore, we used PC12 cells instead and transfected with NPLER$^{NPYfl\text{-}mTq2}$ (Figure 8A) or NPLER$^{NkBfl\text{-}mTq2}$ (Figure 8G), respectively.

NPLER$^{NPY}$ puncta colocalize with DCV markers including ChgA, ChgB, ScgII and ScgIII. All of them label NPLER$^{NPY}$ puncta to some extent, not perfectly ((Figure 8B-E, white triangles: colocalization, arrows: no colocalization). We did not see ScgV staining in PC12 cells (Figure 8F). In comparison, only a small fraction of NPLER$^{NkB}$ puncta colocalize with ChgB (Figure 8I) but not the others (Figure 8H, J,K). The majority of NPLER$^{NkB}$ seem not being labeled by any of the used DCV markers. It is likely that the NkB reporter is routed into a unique group of DCVs that are not labeled by the panel of markers in this study. Alternatively, these puncta may be transported to other cellular organelles like lysosomes. Further investigations using other DCV and organelle markers may help resolve the identity of NPLER$^{NkB}$ routing destinations. Taken together, we conclude that NPLER$^{NPY}$ and NPLER$^{NkB}$ are routed in N46 and PC12 cells, suggesting that these two neuropeptides employ different sorting and trafficking mechanisms.

**Visualizing NPY release with NPRR$^{NPY}$**

Both N46 cells and PC12 cells can release neuropeptides under high potassium conditions (Figure 2D-E) (Chen et al., 1997). We conducted a mini-screen for more physiologically relevant secretagogues based on previous reports in bovine adrenal chromaffin cells (Podvin et al., 2015). The incubation with 100nM Pituitary adenylate cyclase-activating polypeptides (PACAP) in both N46 cells and PC12 cells caused the significantly decrease of anti-NPY fluorescence (Figure 9A-B), indicating the presence and efficiency of PACAP-triggered release of NPY.

Though the expression profiles of neuropeptides are well-characterized in many cell types, it remains largely unknown that how they are released. Our previous work in *Drosophila* (Ding et al., 2019), as well as the success of various similar reporters for imaging synaptic vesicles and secretory

granules (Gandasi et al., 2015; Miesenböck et al., 1998; Rutter et al., 2006), motivated us to generate neuropeptide release reporters (NPRRs) in mammalian cells. The engineering of NPLERs gained us an understanding of proper design of a sorting domain. We then surveyed various pH-sensitive fluorescent proteins and genetically engineered calcium indicators (GECIs) to select a proper reporter domain (Figure 3D). The best candidate CMV-$NPY_{64}$-mVSEP was a combination of a NPY-containing sorting domain and a novel pH sensitive fluorescent protein (Figure $9C_1$). The pH sensitivity profile of mVSEP provided a huge contrast between intravesicular microenvironment (pH=5.5) and extracellular spaces (pH=7.4) (Figure $9C_2$). We named the reporter $NPRR^{NPY}$. KCl-evoked release of $NPRR^{NPY}$ was observed as the brightening of sparse puncta in N46 cells (Figure 9D, orange triangles). The dynamics exhibited a relatively long release phase suggested by the "fat tail" of fluorescence curve (Figure 9E). PACAP-evoked release in N46 cells showed similar pattern (Figure 9F, orange triangles), but the peaks were sharper (Figure 9G). These results collectively suggest that the neuropeptide release dynamics may vary with different stimuli. PACAP-evoked release in PC12 cells (Figure 9H, orange triangles) were not as strong and experienced a rapid decay unlike in N46 cells (Figure 9I). We were surprised by the observation, as PACAP incubation experiments suggested a stronger release in PC12 cells rather than in N46 cells (Figure 9A-B). One explanation is the time scale difference between the incubation experiment (30 mins) and live imaging (90 seconds per trial). While the imaging focused on the puncta with fluorescent change, we observed that a large fraction of fluorescent blobs in PC12 cells remained stable in our imaging trials (Figure 9H). PC12 cells may adopt an asynchronous, slow-release mode. We attempted to prolong the length of recording, yet the weak adherence of PC12 cells gave rise to uncorrectable motion artifacts. Nevertheless, we demonstrated that the NPRR dynamics was dependent on both stimulation protocols and cell types.

**An NPLER-based RNAi screening platform**

RNA interference (RNAi) is a widely recognized approach for sequence-specific silencing via regulating mRNA stability (Wilson & Doudna, 2013). It is used both as a powerful gene knock-down tool in model organisms (Agrawal et al., 2003; Svoboda, 2020), and as a promising therapeutic strategy (Aagaard & Rossi, 2007; Setten et al., 2019). Cell line-based RNAi screen entails selection of a proper cell system and quantitative measurements such as qPCR of a targeted gene. We proposed to facilitate the screening by establishing an NPLER-based platform that (1) visualizes the efficacy of knock-down and (2) establishes a universally applicable cell line.

PC12 cells do not express NkB (Figure 7D$_2$). The introduction of NPLER$^{NkBfl\text{-}mTq2}$, however, showed DCV-like puncta (Figure 7C) which are partially labeled by marker ChgB (Figure 8I), suggesting that at least some NPLER$^{NkB}$ molecules were routed correctly. We therefore designed two siRNAs targeting different regions of NkB gene (Figure 10A), either of which was co-transfected with NPLER$^{NkB}$ (Figure 10B). Cells were double stained with GFP antibody (against the reporter domain of NPLER) and NkB antibody (against the sorting domain of NPLER). We calculated the ratio of NkB staining between the successfully transfected cells and the non-transfected cells. The mean ratios of no siRNA, siRNA$^{Scramble}$ and siRNA$^{NkB\text{-}1}$ are between 1.6-1.8 (1.848, 1.679, 1.677) with no statistically significant differences, while the ratio in siRNA$^{NkB\text{-}2}$ (1.149) is significantly lower in siRNA$^{Scramble}$ control (Figure 10C)), suggesting the high efficiency of NkB knock-down by siRNA$^{NkB\text{-}2}$. We reasoned that the siRNA interrupted the NPLER expression via targeting its NkB fragment in the sorting domain, by which the reporter domain would too be affected. We further quantified the fluorescent intensity of reporter domain of transfected cells. The reporter domain fluorescence in siRNA$^{NkB\text{-}2}$ is significantly lower than in control group, consistent with the findings

in NkB staining. NPLER$^{NkB}$-PC12 cell system provides a prototypical model for initial RNAi screening to an exogenous neuropeptide with a well-established cell line. It is possible that such practice is universally applicable to other neuropeptides.

**Discussion**

Here we described the development of two collections of sister reporters, NPLERs (Neuropeptide Localization and Expression Reporter) and NPRRs (Neuropeptide Release Reporter). Proof-of-concept experiments with NPLERs against NPY and NkB reveal their differences in sorting and routing. N46, a novel embryonic hypothalamic cell line, as well as the canonical PC12 cells, were used as testbeds for the reporters (Table 1). This allowed us to uncover previously unexplored cell type specificity in terms of neuropeptide processing. We further visualized NPY release dynamics in response to PACAP, a physiologically relevant stimulus and showed the distinct properties of release in N46 and PC12 cells. Lastly, we transformed PC12 cells to a potentially generalizable RNAi screening platform by introducing an NPLER for an exogenous neuropeptide. These results collectively contribute to a deeper understanding of neuropeptide pathways, and provide a powerful model platform to facilitate the explorations of neuropeptide-targeting therapeutics.

Though we provide compelling evidence on the proper sorting and trafficking of these reporters, it is likely that their strong expression may cause protein overload in the secretory pathways. Transfection of NPLER$^{NPY}$ candidates in cells that endogenously express NPY sometimes result in a perinucleus “cap” (Figure 5), a phenomenon not observed with NPLER$^{NkB}$. Given that NkB was relatively sparse in compared to NPY in N46 cells (Figure 2A) and showed no staining in PC12 cells (Figure 7D), it is possible that the NPLER$^{NPY}$ is competing with endogenous NPY for the secretory

capacities. Detailed mechanisms are unknown and await further investigations. A potential solution to this problem is to employ knock-in techniques such as CRISPR-Cas9 (Doudna & Charpentier, 2014; Hsu et al., 2014) to insert the reporter to a genetic locus to fine-tune the expression to an appropriate level.

We also attempted to image NkB release but failed due to their low baseline expression. Unlike NPLER$^{NkB}$ that are compatible with immunocytochemistry to amplify the fluorescent intensity, NPRRs are designed for live imaging that entails higher baseline fluorescence for the identification of puncta. The use of high laser power bleached the fluorophores and hindered long-term imaging. A new fluorescent protein with optimized pH sensitivity, brightness and better resistance to photobleaching will be pivotal to the next-generation NPRR. Moreover, we failed to generate the red version of NPRRs due to the failure of capturing fluorescent contrast. New pH-sensitive red fluorescent proteins will be a powerful addition to the NPRR collection. An ideal yet undone experiment is to simultaneously image NPY and NkB release, and track their fluorescent change to multiple types of stimuli. It is tempting to investigate if the routing differences unveiled by the NPLER studies also lead to any differences in release dynamics.

We also exploited the use of NPLERs for RNAi screening by integrating NPLER$^{NkB}$ to PC12 cells, which do not endogenously express NkB. It is shown that the efficacy of siRNA could be visualized with NPLER brightness, and PC12 cells may function as a generic testbed for an exogenous neuropeptide. These advantages may accelerate large-scale, imaging-based neuropeptide siRNA screening. Though we are too aware of its relatively low sensitivity in relation to the traditional RT-

PCR approach, which is reasonable due to the differences in the amplification process. We still believe that the imaging-based platform serves as an alternative strategy for preliminary screenings.

In the long term, we hope that NPLER/NPRR platform will better the understanding of neuropeptide biology. Its *in vivo* applications will uncover the dynamic neuromodulation of behaviorally and physiologically relevant neural circuits. The platform may ultimately work as a hypothesis generator for the discoveries of novel therapeutics for treating human diseases.

**A**

RT-PCR results (from suppliers)

| | Hypothalamic | | | | | Insulinoma |
|---|---|---|---|---|---|---|
| | mHypoE-N7 | mHypoE-N46 | mHypoA-2/29 | mHypoA-2/32 | mHypoA-59 | MIN6beta |
| NPY | - | + | + | - | ++ | ? |
| NkB | ++ | ++ | very weak | strong | - | ? |
| Insulin | - | + | - | - | - | ++ |

**B**

IHC results

| | Hypothalamic | | | | | Insulinoma |
|---|---|---|---|---|---|---|
| | mHypoE-N7 | mHypoE-N46 | mHypoA-2/29 | mHypoA-2/32 | mHypoA-59 | MIN6beta |
| NPY | very weak/- | + | weak | - | + | + |
| NkB | strong | + | weak | + | + | weak |
| Insulin | - | very weak | - | - | very weak/- | ++ |

**C**


**D₁**

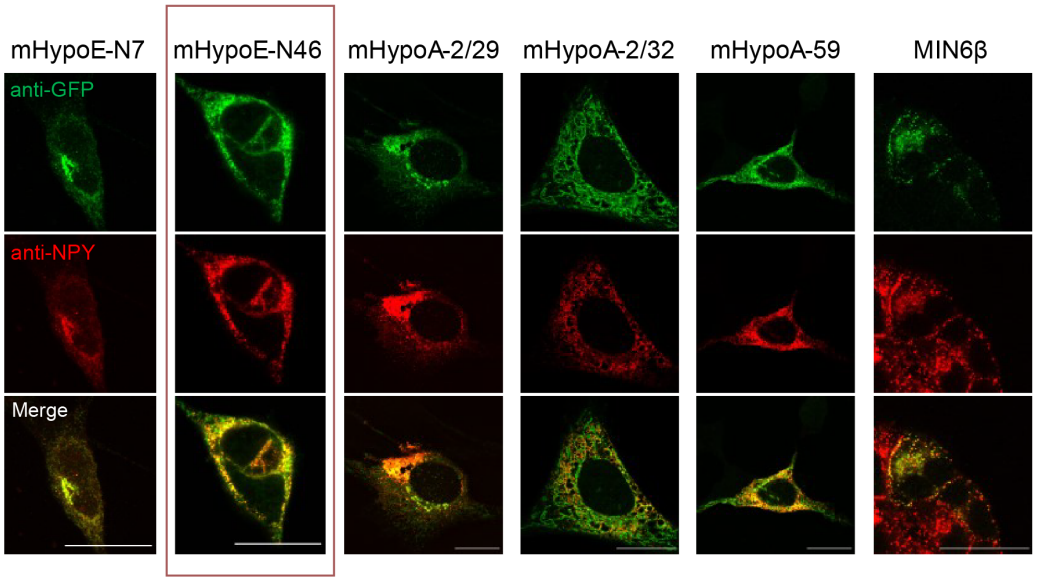


**D₂**

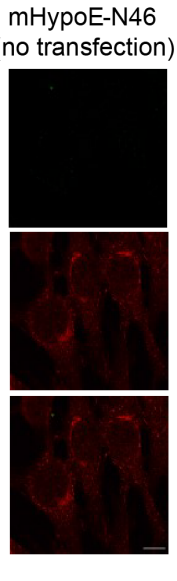


**Figure 1: A novel cell line for design, screening, and validation of neuropeptide reporters.**

**(A)** RT-PCR profiles were used as references to shortlist a collection of hypothalamic cell lines to study the neuropeptides of interest (details in Introduction); an insulinoma cell line was acquired in parallel due to its popularity in neuropeptide research (Gandasi et al., 2015; Makhmutova et al., 2017; Varadi et al., 2005). **(B)** Antibody staining-based screening of candidate cell lines yield similar results as in RT-PCR experiments yet provide extra neuropeptide expression profile in insulinoma cells. **(C,D$_1$)** Expression pattern screening of candidate cell lines with a fiduciary neuropeptide reporter NPLER$^{NPYfl\text{-}GFP}$ that follows similar design as human NPY-GFP (see **Materials and Methods** for details). **(D$_2$)** is a no-transfection control for mHypoE-N46. GFP/NPY double staining of cell lines result in a good candidate mHypoE-N46 (highlighted in red box, "N46" is used in the following contexts), which shows 1) fluorescent puncta and 2) perfect colocalization of NPLER and NPY staining pattern, both highly suggestive of proper neuropeptide trafficking. Scale bar, 10 μm.

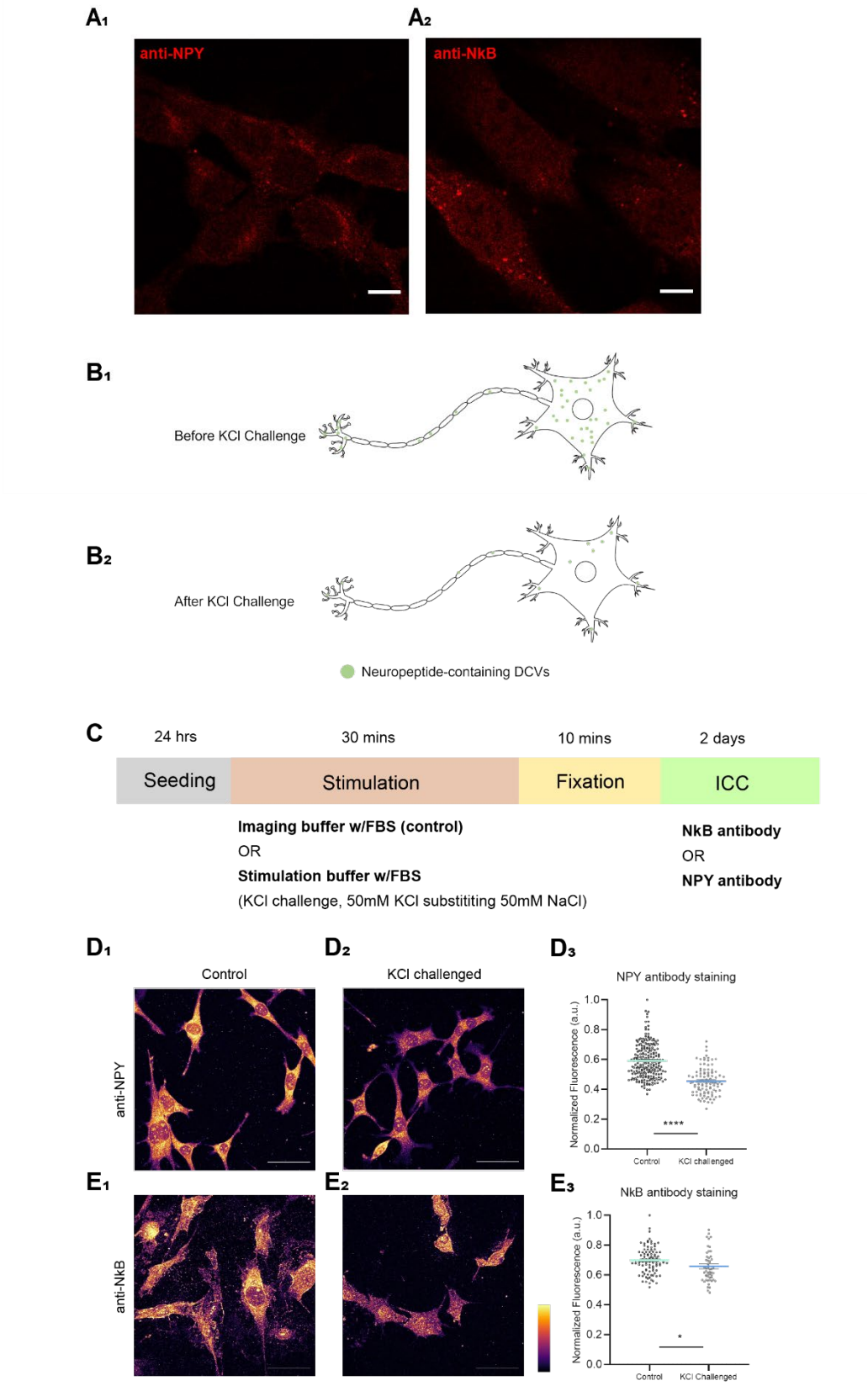


**Figure 2: N46 cells express and release NPY and NkB.**

**($A_1$)** NPY and **($A_2$)** NkB staining of N46 cells. **(B)** KCl-stimulation model. KCl challenge strongly depolarizes the cells and triggers massive neuropeptide release. Neuropeptide-containing DCVs in the control cells **($B_1$)** will be mobilized, primed and released by KCl stimulation **($B_2$)**. **(C)** Experimental procedure for KCl challenge experiment. N46 cells were seeded and grown for 24 hours, following incubation in FBS-supplemented buffer or stimulation buffer (with 50mM $K^+$ replacing 50mM $Na^+$) for 30 minutes. Cells were subsequently fixed and stained with neuropeptide antibody. **(D)** NPY staining of control **($D_1$)** and KCl challenged **($D_2$)** N46 cells. Quantification **($D_3$)** show statistically significant reduction of NPY signals in KCl challenged group (N=102-224), implying the cells release endogenous NPY upon strong activation. **(E)** NkB staining of control **($E_1$)** and KCl challenged **($E_2$)** N46 cells. Quantification **($E_3$)** reaches similar conclusions (N=53-96) as in **($D_3$)**. (*P<0.05, ****P<0.0001, Mann-Whitney *U* test). Images in **($D_1$, $D_2$, $E_1$, $E_2$)** were normalized and pseudo-colored to highlight contrasts.

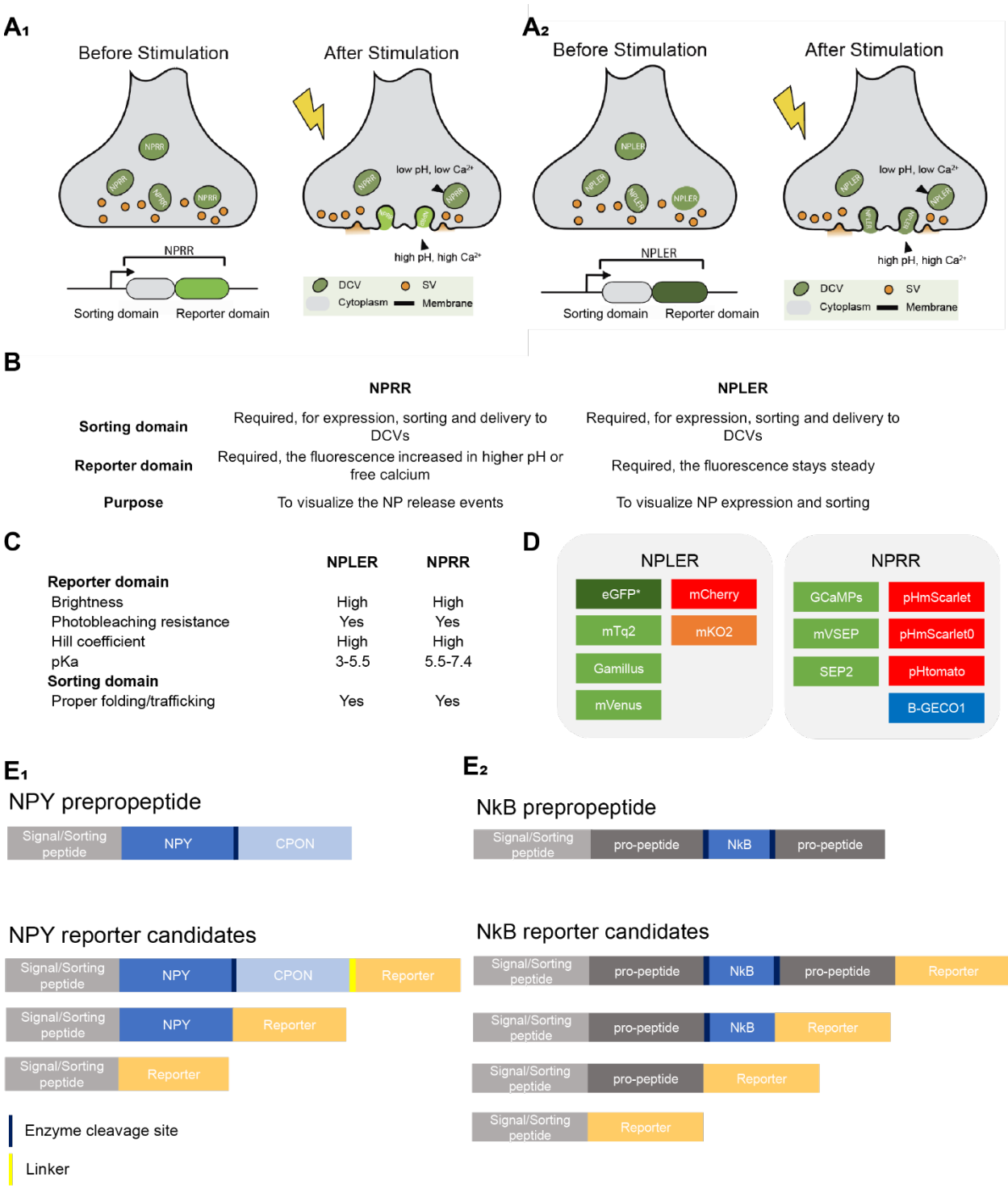


**Figure 3: Neuropeptide Localization and Expression Reporters (NPLERs) and Neuropeptide Release Reporters (NPRRs).**

**($A_1$)** Principles of Neuropeptide Release Reporter (NPRR), adapted from studies in Chapter 2 (Ding et al., 2019; Han & Ding, 2022), **($A_2$)** Principles of Neuropeptide Localization and Expression Reporter (NPLER). **(B)** Summary of similarities and contrasts between NPRR and NPLER. The design of sorting domain is interchangeable. The choice of reporter domain and design purposes are different. **(C)** Rationales of reporter domain selection were used to comply with principles in **(B)**. **(D)** Candidate reporter domains were selected based on **(C)**. **(E)** Candidate sorting domains were designed following the mapping of neuropeptide prepropeptide domains, the concatenation of reporter domain to the C terminus was an empirical inference from the *Drosophila* screening (Ding et al., 2019). Candidate reporters were generated for two neuropeptides of interest, Neuropeptide Y (NPY) **($E_1$)** and Neurokinin B **($E_2$)**.

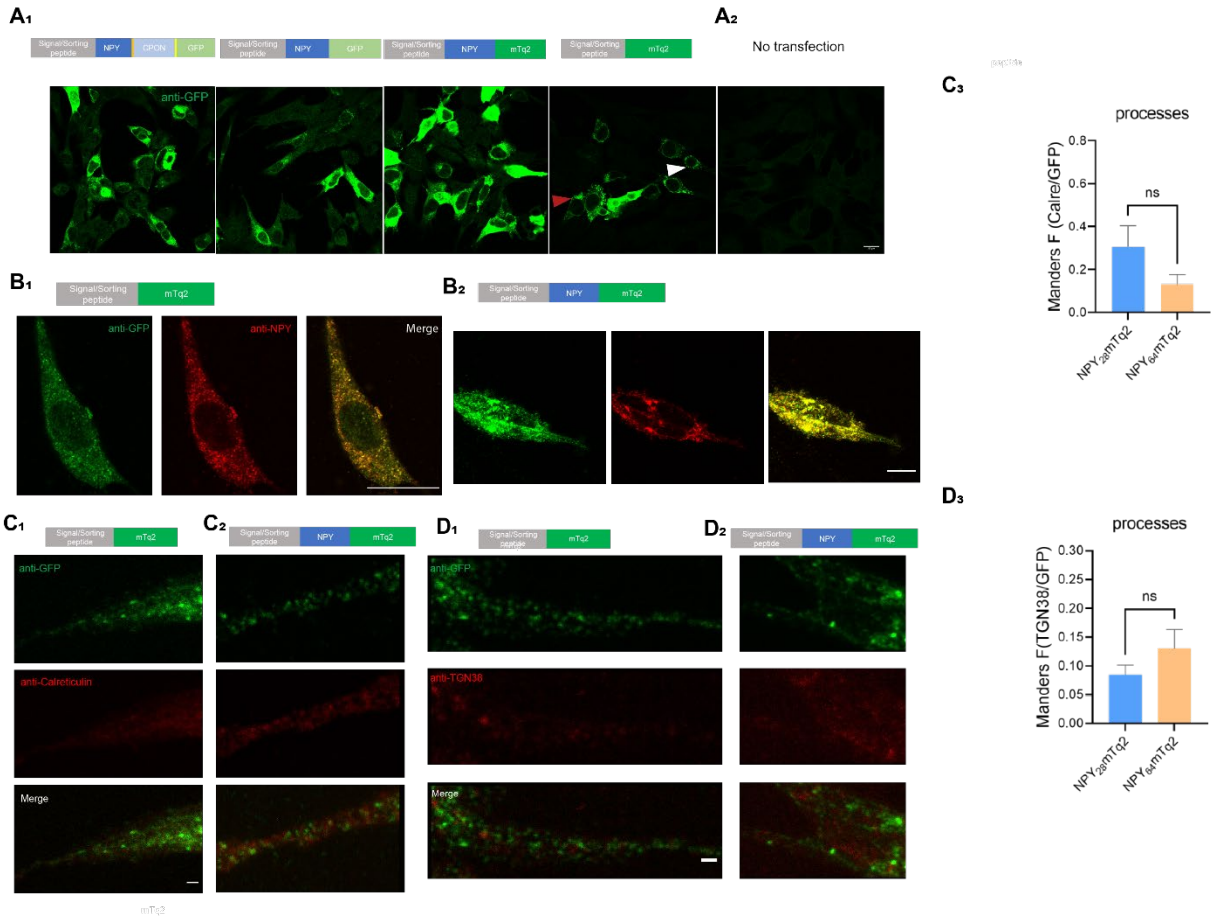


**Figure 4: Comparison of NPLER$^{NPY}$ candidates with variations in the sorting domain.**

**(A)** Comparisons between NPLER$^{NPY}$ with various configurations of sorting domains ($A_1$) and non-transfected blank control ($A_2$). Red triangle points to a cell with perinucleus accumulation, white triangle points to a cell without. **($B_1$)** Configuration of NPLER$^{NPY28\text{-}mTq2}$ (CMV-$NPY_{28}$-mTq2). Transfected N46 cells show perfect colocalization of NPLER$^{NPY28\text{-}mTq2}$ and NPY, note that the reporter transgene does not contain NPY fragment. NPY staining signals are completely contributed by endogenous NPY. **($B_2$)** Configuration of NPLER$^{NPY64\text{-}mTq2}$ (CMV-$NPY_{64}$-mTq2), transfected N46 cells show perfect colocalization of NPLER$^{NPY64\text{-}mTq2}$ and NPY, note that the reporter transgene contains the antigen reactive to NPY antibody. Scale bar, 10 µm. **($C_{1\text{-}2}$)** GFP/Calreticulin double-labeling of NPLER$^{NPY28\text{-}mTq2}$ transfected cell, similarly for NPLER$^{NPY64\text{-}mTq2}$, **($C_3$)** Comparison of overlap between Calreticulin and GFP immunofluorescence in NPLER$^{NPY64\text{-}mTq2}$ and NPLER$^{NPY28\text{-}mTq2}$ (N=7-8, ns: not significant, Mann-Whitney *U* test). **($D_{1\text{-}2}$)** GFP/TGN38 double-labeling of NPLER$^{NPY28\text{-}mTq2}$ transfected cell, similarly for NPLER$^{NPY64\text{-}mTq2}$, **($C_3$)** Comparison of overlap between TGN38 and GFP immunofluorescence in NPLER$^{NPY64\text{-}mTq2}$ and NPLER$^{NPY28\text{-}mTq2}$ (N=13-14, ns: not significant, Mann-Whitney *U* test).

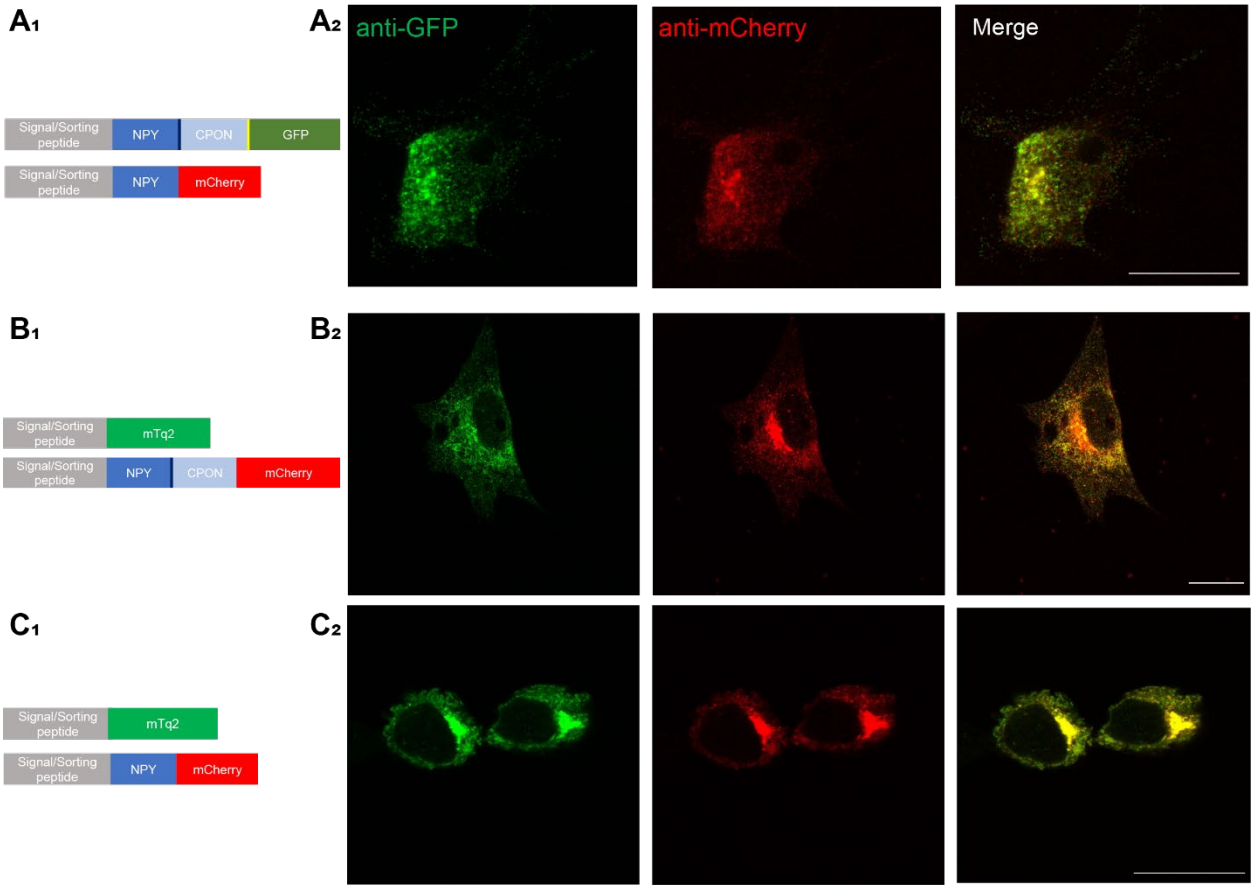


**Figure 5: NPLER$^{NPY}$ candidates with various sorting domains show similar subcellular pattern.**

Green and red NPLERs with different sorting domains were co-transfected in several ways. **($A_1$, $B_1$, $C_1$)** illustrate transgenes used for transfection in **($A_2$, $B_2$, $C_2$)**. Comparisons of green and red channels in **($A_2$, $B_2$, $C_2$),** respectively, show similar subcellular patterns. Scale bar, 10 µm.

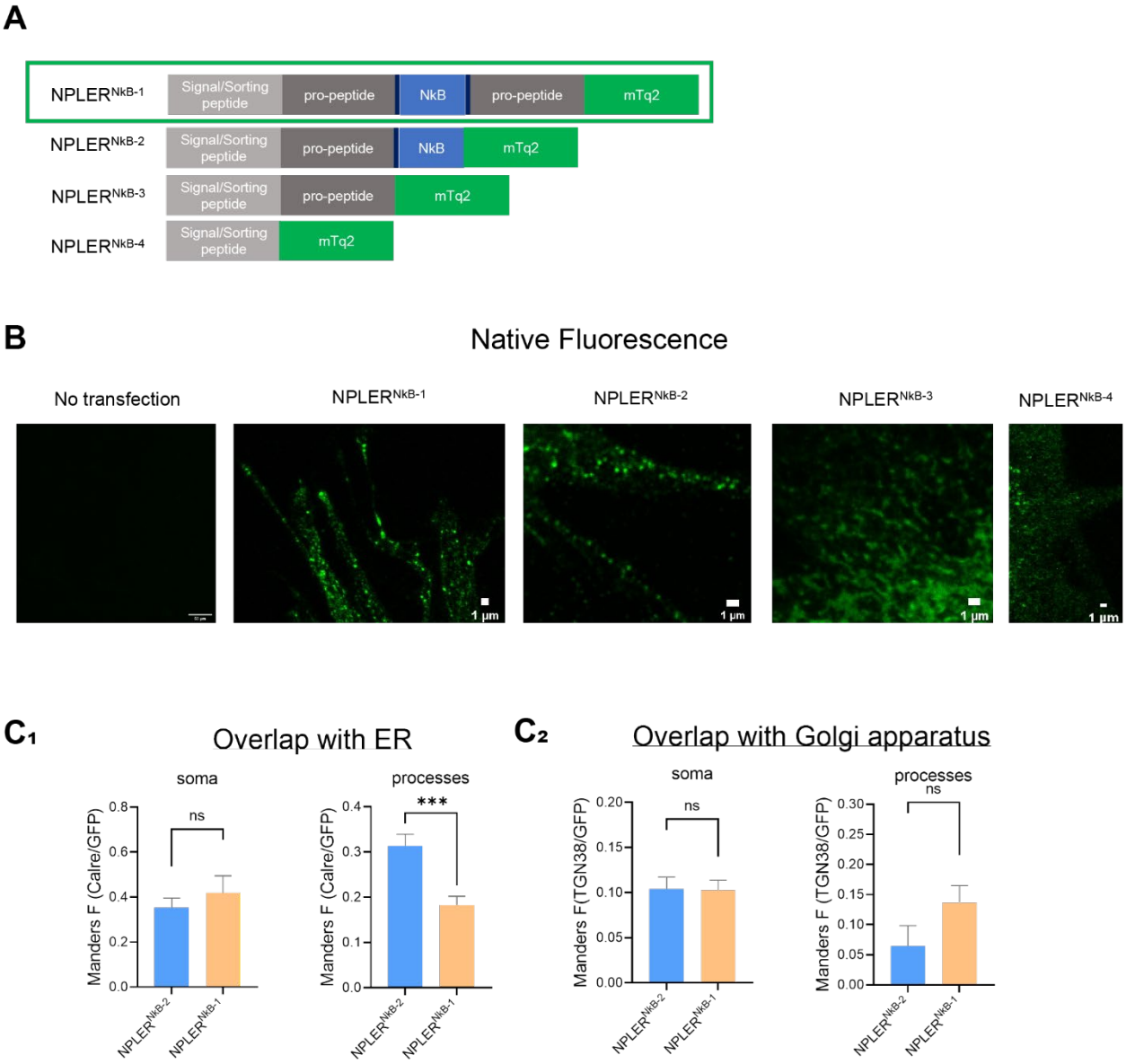


**Figure 6: NPLER$^{NKB}$ reporter requires full-length sorting domain for optimal performance.**

**(A)** Illustration of various designs of NPLER$^{NkB}$ candidates, which differ in the configuration of sorting domains. The best candidate full-length version NPLER$^{NkB-1}$ is highlighted in green box. **(B)** Native fluorescence screening of NPLER$^{NkB}$ candidates in N46 cells. NPLER$^{NkB-1}$ and NPLER$^{NkB-2}$ exhibit fluorescent puncta in the processes that suggest proper vesicular trafficking, while NPLER$^{NkB-3}$ and NPLER$^{NkB-4}$ do not. Scale bar, 1 µm except in control (10 µm). **(C)** Further comparisons between NPLER$^{NkB-1}$ and NPLER$^{NkB-2}$ were assisted by double labeling with an ER marker (Calreticulin) or a golgi marker (TGN38). Overlaps between the reporter and the organelle marker were quantified with the Manders' overlap coefficients. NPLER$^{NkB-2}$ show higher level of overlap with ER, suggesting higher ER retention and lower efficiency of trafficking. Data are plotted as mean±s.e.m. (***P<0.001, Student's t-test).

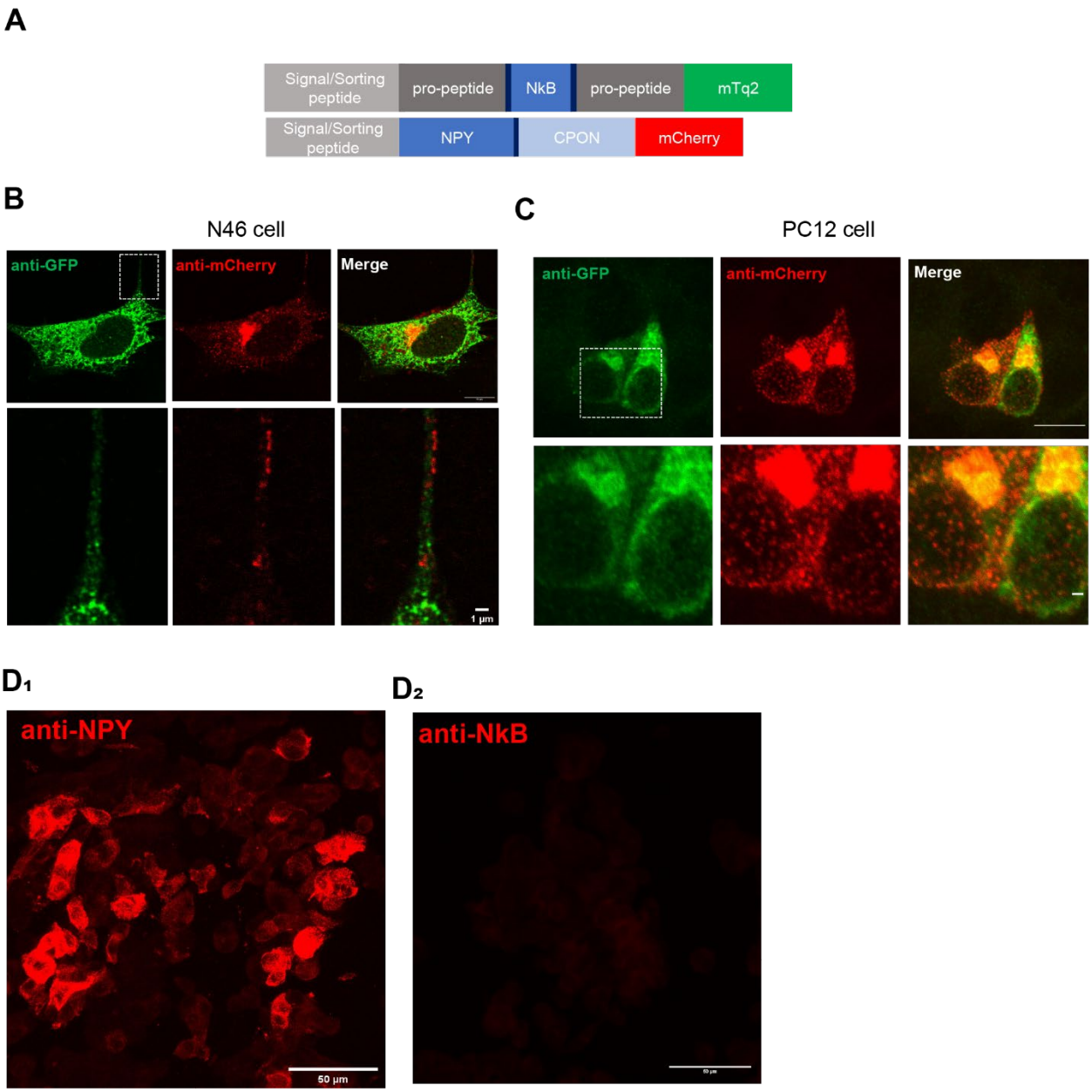


**Figure 7: NPLER$^{NPY}$ and NPLER$^{NkB}$ are routed differently in N46 and PC12 cells.**

**(A)** Illustration of NPLER$^{NkB\text{-}1}$ (CMV-NkB$_{full}$-mTq2) and NPLER$^{NPYfl\text{-}mCherry}$ (CMV-NPY$_{full}$-mCherry). They were co-transfected in the cell line for experiments in **(B,C)**. **(B)** Two-color staining of co-transfected N46 cells. NPLER$^{NkB\text{-}1}$ and NPLER$^{NPYfl}$ show different subcellular patterns (upper) and do not colocalize in the processes (lower). **(C)** Two-color staining of co-transfected PC12 cells, with similar observations in **(B)**. Scale bar, 10 µm (upper) and 1 µm (lower). **(D)** PC12 cells express endogenous NPY **(D$_1$)** but not NkB **(D$_2$)**. Scale bar, 50 µm

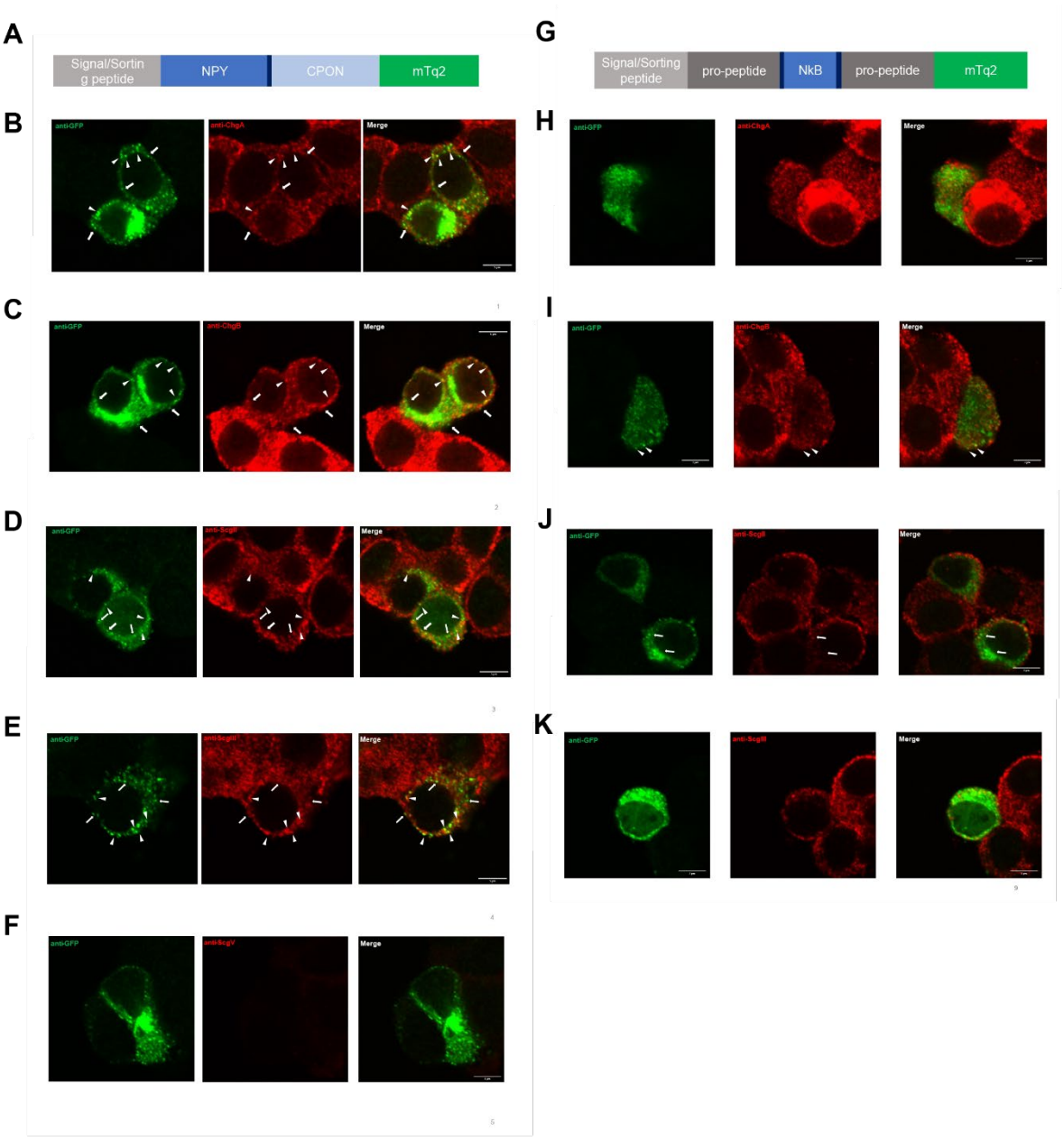


L

| | ChgA | ChgB | ScgII | ScgIII | ScgV |
|---|---|---|---|---|---|
| PC12 cell | + | + | + | + | - |
| **Overlap** | | | | | |
| NPY⁺ DCV | + | + | + | + | N/A |
| NkB⁺ DCV | - | + | - | - | N/A |

**Figure 8: Difference in DCV entry of NPLER$^{NPY}$ and NPLER$^{NkB}$ in PC12 cells.**

**(A)** Illustration of NPLER$^{NPYfl\text{-}mTq2}$ (CMV-NPY$_{full}$-mTq2). PC12 cells transfected with **(A)** were fixed and co-stained, respectively, with multiple canonical DCV markers, including Chromogranin A **(B)**, Chromogranin B **(C)**, Secretogranin II **(D)**, Secretogranin III **(E)** and Secretogranin V **(F)**. Similarly, PC12 cells transfected with NPLER$^{NkB\text{-}1}$ (CMV-NkB$_{full}$-mTq2, illustrated in **(G)**) were co-stained with the same panel of DCV markers **(H-K)** except Secretogranin V, as it showed no expression in PC12 cells **(F)**. White triangles indicate colocalization of DCV markers with NPLERs, yet white arrows point to NPLER fluorescent not labeled by a DCV marker. Scale bar, 50 μm. **(L)** summarizes the presence/absence of DCV markers in PC12 cells, as well as the presence of their overlap with NPY and NkB NPLERs, respectively.

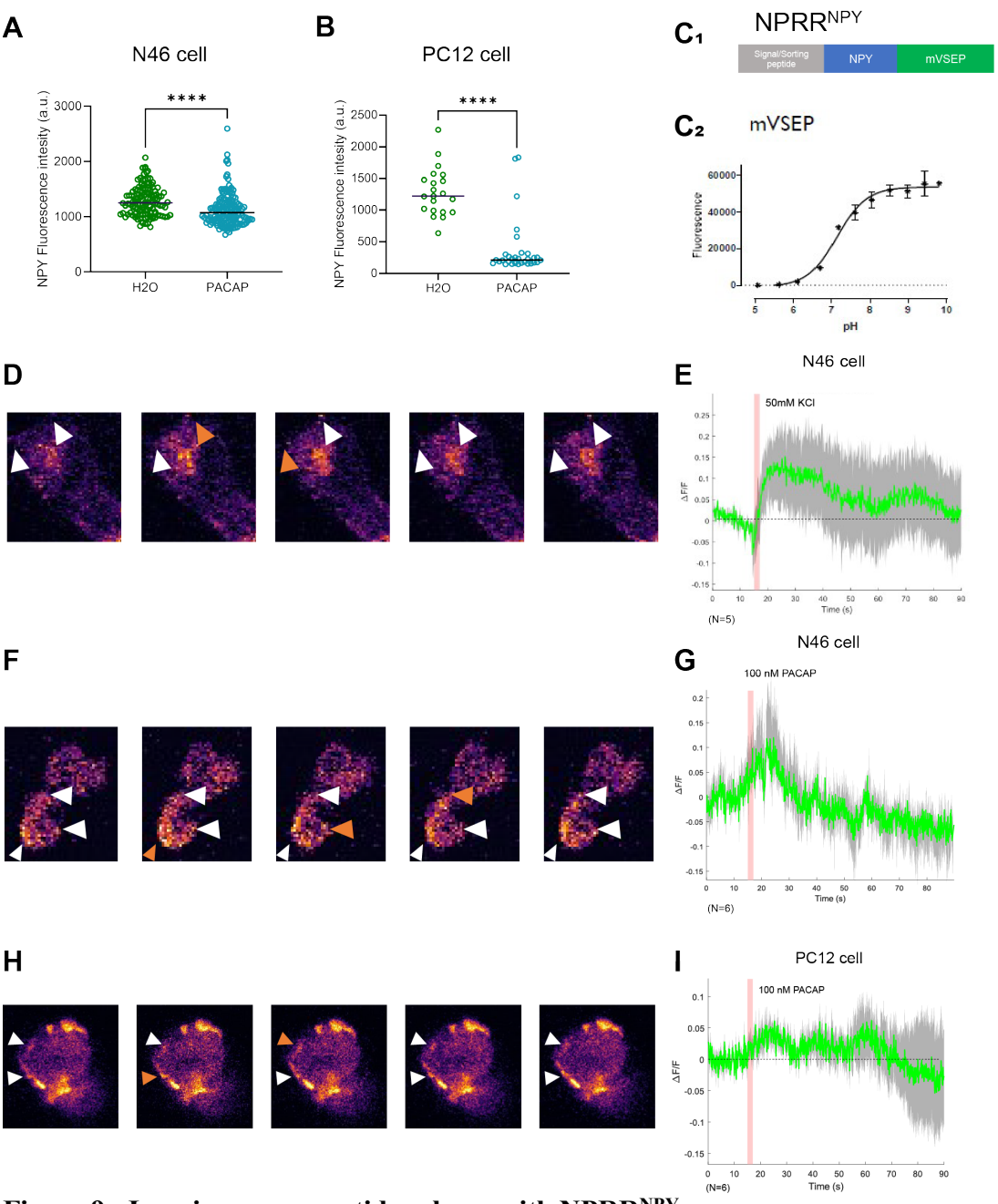


**Figure 9: Imaging neuropeptide release with NPRR$^{NPY}$.**

**(A-B)** Cells treated with 30 min incubation in either solvent ($H_2O$) or 100 nM PACAP were fixed and used for NPY antibody staining, the fluorescent intensity of each cell was individually measured, both in **(A)** N46 (N=121-134) and **(B)** PC12 (N=21-31). Data were pooled for comparison (****P<0.0001, Mann-Whitney *U* test). **(C1)** Illustration of NPRR$^{NPY}$ configuration. **(C2)** Characterization of a novel pHluorin mVSEP that constitutes the reporter domain of NPRR$^{NPY}$. Similar case was seen in PC12 cells. N46 cells transfected with NPRR$^{NPY}$ were imaged with KCl stimulation **(D-E)** or PACAP stimulation **(F-G)**, similarly transfected PC12 cells were imaged with

PACAP stimulation **(H-I)**, KCl stimulation caused PC12 cells dislodge and hindered live imaging. Images in **(D,F,H)** are pseudo-colored to highlight contrast. Triangles point to regions of interest, while orange triangles indicate the onset of releasing events.In **(E,G,I)**, red bar indicates the introduction of stimuli, pooled trials are presented as mean±s.e.m. (N=5-6, shown in figures).

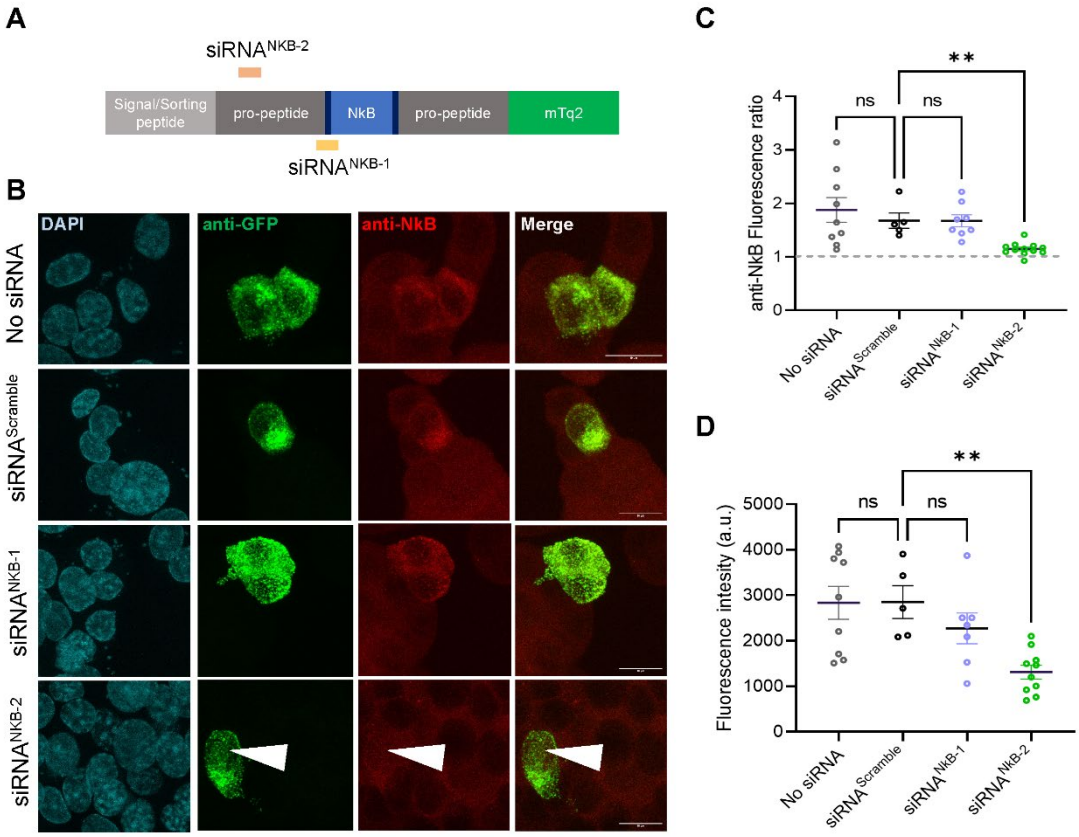


**Figure 10: An NPLER-based RNAi screening platform.**

**(A)** The targeting regions of NkB siRNAs, in reference to the NPLER$^{NkB-1}$. **(B)** 3-color confocal imaging of PC12 cells transfected with siRNAs. All groups show positive correlation of GFP channel and NkB channel except in siRNA$^{NkB-2}$. White arrows point to a representative cell that shows NkB reduction when transfected, suggesting the knock-down effect of NkB by the siRNA. **(C)** Images were quantified in each group to compare the anti-NkB fluorescence ratio between NPLER transfected or non-transfected cells in the same experiment. The ratio of siRNA$^{NkB-2}$ is statistically lower than the siRNA$^{Scramble}$ (N=5-12) **(D)** The absolute fluorescent intensity of transfected cells was quantified and compared for each group (N=5-10) (**P<0.01, Kruskal-Wallis test).

| | Origin | Growth | Maintenance | Adherence | Transfection efficiency* | Expression of NP | Prescence of DCV |
|---|---|---|---|---|---|---|---|
| N46 | Mouse embryonic hypothalamic cell | Fast | Easy | High | 10-20% | Yes | ? |
| PC12 | Rat pheochromocytoma cell | Slow | Hard | Low | 5-10% | Yes | Yes |

**Table 1: Comparison of N46 cells and PC12 cells.**

## Materials and Methods

### Cell culture

Hypothalamic cell lines (Cedarlane Laboratories), MIN-6β cells (Addexbio Technologies) and PC12 cells (ATCC) were maintained at 37 ℃ under 5% $CO_2$. Hypothalamic cell lines were maintained in high-glucose Dulbecco's modified essential medium containing 10% fetal bovine serum, 100 units/ml penicillin, and 0.1 mg/ml streptomycin as suggested by the cell line supplier. MIN-6β cells were maintained similarly except 15% fetal bovine serum was added. PC12 cells were grown in Dulbecco's modified essential medium containing 5% calf serum, 5% horse serum, 100 units/ml penicillin, and 0.1 mg/ml streptomycin. In every passage, a fraction of cells was stored in liquid nitrogen for further use. All cells were discarded after 10 times of passage. JetPRIME® Versatile DNA/siRNA transfection reagent (Polyplus transfection) was used in all cell transfection experiments.

### Molecular cloning

All PCR reactions were performed using PrimeSTAR HS DNA polymerase (Takara #R045Q). To construct NPRR and NPLER candidates, sorting domain fragments were cloned from mouse cDNA library (OriGene Technologies) or synthesized using gBlocks service (Integrated DNA Technologies), while reporter domains were cloned from commercially available plasmids that contain DNA fragments encoding fluorescent proteins (Addgene). Human NPY-GFP (Addgene #74629) was used as a reference transgene. All fragments were subcloned into pCMV or pAAV backbone using Gibson Assembly approach. All constructs were verified via DNA sequencing (Laragen). Candidate plasmids that pass preliminary cell line screening underwent Maxiprep, pCMV plasmids were prepared with Pureyield System (Promega A2393) and pAAV plasmids with Nucleobond® Xtra Maxi EF (Takara #740424.10).

**Immunocytochemistry (ICC)**

Cells were seeded in 24-well plates that were prepared in advance to have a piece of poly D-lysine (PDL) coated cover glass (Carolina Biological Supply 633029) that were in each well. After 24 hours of transfection, cells were quickly rinsed with PBS and fixed in 4 % paraformaldehyde for 10 min at room temperature. After two 5-min rinses with PBS and one 5-min rinse with 0.1% PBST, cells were blocked for 3 minutes in PBST with 5% normal goat serum, and subsequently incubated in primary antibodies overnight at 4 °C with gentle shaking. Following three 10-min rinses with PBS, cells were incubated in secondary antibodies for 2 hours at room temperature with gentle shaking. Cover glasses with cells on top were carefully dried with Kimwipe and inverted placed on a slide with a tiny drop of mounting media (Vectashield with DAPI, Vector Laboratories; Slowfade, Thermo Scientific S36963). To prevent cover glasses from gliding, electric tapes were cut in tiny strips and placed on both sides of the glass. Confocal serial optical

sections were acquired using an Fluoview FV3000 Confocal laser scanning biological microscope (Olympus) with a 60×, 1.30 N.A. silicone oil objective (Olympus). All image processing and analyses were performed using ImageJ (National Institute of Health).

The following primary antibodies were used: Chicken anti-GFP (1:2000, Aveslab #1020), Rabbit anti-NkB (1:500, Thermo Scientific PA116745), Rabbit anti-NPY (1:500, BMA Biomedicals T4070), Mouse anti-dsRed (1:500, Takara #632543), Rabbit anti-dsRed (1:500, Takara #632496), Rabbit anti-NPY (1:500, BMA Biomedicals T4070), Rabbit anti-NPY (1:500, Cell Signaling Technology 11976S), Rabbit anti-ChgA (1:500, SYSY #259003), Rabbit anti-ChgB (1:500, SYSY #259103), Rabbit anti-ScgII (1:500, Proteintech 20357-1-AP) , Rabbit anti-ScgIII (1:500, Proteintech 10954-1-AP), Rabbit anti-ScgV (1:500, Proteintech 10761-1-AP), Rabbit anti-Calreticulin (1:500, Novus Biologicals NB600-103SS), Rabbit anti-TGN38 (1:500, Novus Biologicals, #NBP1-03495SS), Mouse anti-TGN38 (1:500, BD #610898).

The following secondary antibodies were used: Alexa Fluor 488 Goat anti-Chicken IgY (#A11039, Invitrogen), Alexa Fluor 488 Goat anti-Rabbit IgG (#A11008, Invitrogen), Alexa Fluor 568 Goat anti-Rabbit IgG(H+L) (#A11011, Invitrogen), Alexa Fluor 568 Goat anti-Mouse IgG(H+L) (#A11004, Invitrogen) and Alexa Fluor 633 Goat anti-Mouse IgG(H+L) (#A21050, Invitrogen).

**RNAi experiments**

All siRNA probes were purchased or synthesized (Integrated DNA Technologies), and transfected using JetPRIME® Versatile DNA/siRNA transfection reagent (Polyplus transfection) to yield the final concentration of 50 μM. Transfection efficiency was estimated with fluorescently labeled TYE

563 siRNA control provided (Integrated DNA Technologies) prior to each batch of experiments. $siRNA^{Scramble}$ was a negative control from the same supplier. Antisense sequences of used siRNA are shown below.

$siRNA^{NkB-1}$: ACGUUUCUGUGGAAGUGAUGUCUCCUU

$siRNA^{NkB-2}$: AAGCUGAGGGCGAGGACAGCCGCAAAC

**Live imaging**

Cells were seeded in 24 well plates that were prepared in advance to have 2-3 pieces of PDL-coated cover glass (Warner Instruments 64-0700, 64-0720) placed in each well. After 24-34 hour of transfection, cover glasses were transferred to a customized perfusion chamber and bathed in imaging solutions. The imaging solution used for imaging experiments of hypothalamic cell lines consisted of (in mM): 140 NaCl, 4 KCl, 2 $CaCl_2$, 1 $MgCl_2$, 10 glucose, and 10 HEPES at pH 7.3 as in (Belsham et al., 2004). stimulation solution consisted of (in mM): 94 NaCl, 50 KCl, 2 $CaCl_2$, 1 $MgCl_2$, 10 glucose, and 10 HEPES at pH 7.3 was used for KCl stimulation. Imaging solution for PC12 cell lines contains (in mM):130 NaCl, 5 KCl, 0.33 $Na_2HPO_4$, 0.44 $KH_2PO_4$, 4.2 $NaHCO_3$, 5.6 glucose, 0.8 $MgCl_2$, and 10 HEPES at pH 7.4 as in (Bauerfeind et al., 1995). KCl stimulation of PC12 was performed with imaging solution altered with (in mM) 85 NaCl, 50 KCl, all else equal. Perfusion of imaging and stimulation solution was assisted with a peristaltic pump (Cole-Parmer EW-78001-72), while secretagogue PACAP (Tocris, #1186), was prepared at 1000X concentration (100 nM) and injected locally into the imaging solution. Time-lapse images were acquired using an Fluoview FV3000 Confocal laser scanning biological microscope (Olympus) with a 60×, 0.90 N.A. water objective (Olympus). Resonant scanning mode was used, sampling speed was tuned to 8-10Hz with adjustments in number of averaging, zoom-in factors and size of

imaging window. Image J Plugins including Image Stabilizer (K. Li, CMU) and Template Matching (Q. Tseng) were used for compensating minor x-y drifting. Image series with z-drift were discarded.

**Statistical analysis**

All data analysis was performed with Graphpad Prism 9, Microsoft Excel and custom Matlab codes. Mann-Whitney *U* test was used for comparison in most cases. Data underwent normality tests in advance if parametric comparisons were needed (Kolmogorov-Smirnov test, Shapiro-Wilk test, D'Agostino & Pearson test). Bonferroni correction was used for multiple comparisons.

**References**


Aagaard, L., & Rossi, J. J. (2007). RNAi therapeutics: Principles, prospects and challenges. *Advanced Drug Delivery Reviews*. https://doi.org/10.1016/j.addr.2007.03.005

Agrawal, N., Dasaradhi, P. V. N., Mohmmed, A., Malhotra, P., Bhatnagar, R. K., & Mukherjee, S. K. (2003). RNA Interference: Biology, Mechanism, and Applications. *Microbiology and Molecular Biology Reviews*, *67*(4), 657–685. https://doi.org/10.1128/mmbr.67.4.657-685.2003

Bauerfeind, R., Jelinek, R., & Huttner, W. B. (1995). Synaptotagmin I- and II-deficient PC12 cells exhibit calcium-independent, depolarization-induced neurotransmitter release from synaptic-like microvesicles. *FEBS Letters*, *364*(3), 328–334. https://doi.org/10.1016/0014-5793(95)00419-A

Belsham, D. D., Cai, F., Cui, H., Smukler, S. R., Salapatek, A. M. F., & Shkreta, L. (2004). Generation of a Phenotypic Array of Hypothalamic Neuronal Cell Models to Study Complex Neuroendocrine Disorders. *Endocrinology*, *145*(1), 393–400. https://doi.org/10.1210/EN.2003-0946

Bulgari, D., Jha, A., Deitcher, D. L., & Levitan, E. S. (2018). Myopic (HD-PTP, PTPN23) selectively regulates synaptic neuropeptide release. *Proceedings of the National Academy of Sciences of the United States of America*, *115*(7), 1617–1622. https://doi.org/10.1073/pnas.1716801115

Cavadas, C., Silva, A. P., Cotrim, M. D., Ribeiro, C. A. F., Brunner, H. R., & Grouzmann, E. (2002). Differential secretion of catecholamine and neuropeptide Y in response to KCl from mice chromaffin cells. *Annals of the New York Academy of Sciences*, *971*, 335–337. https://doi.org/10.1111/j.1749-6632.2002.tb04489.x

Chen, T. W., Wardill, T. J., Sun, Y., Pulver, S. R., Renninger, S. L., Baohan, A., Schreiter, E. R., Kerr, R. A., Orger, M. B., Jayaraman, V., Looger, L. L., Svoboda, K., & Kim, D. S. (2013). Ultrasensitive fluorescent proteins for imaging neuronal activity. *Nature*, *499*(7458), 295–300. https://doi.org/10.1038/nature12354

Chen, X., Dimaggio, D. A., Han, S. P., & Westfall, T. C. (1997). Autoreceptor-induced inhibition of neuropeptide Y release from PC-12 cells is mediated by Y2 receptors. *American Journal of Physiology - Heart and Circulatory Physiology*, *273*(4 42-4). https://doi.org/10.1152/ajpheart.1997.273.4.h1737

De Camilli, P., & Jahn, R. (1990). Pathways to regulated exocytosis in neurons. *Annual Review of Physiology*, *52*(1), 625–645. https://doi.org/10.1146/annurev.ph.52.030190.003205

de Juan-Sanz, J., Holt, G. T., Schreiter, E. R., de Juan, F., Kim, D. S., & Ryan, T. A. (2017). Axonal Endoplasmic Reticulum Ca2+ Content Controls Release Probability in CNS Nerve Terminals. *Neuron*, *93*(4), 867-881.e6. https://doi.org/10.1016/j.neuron.2017.01.010

Ding, K., Han, Y., Seid, T. W., Buser, C., Karigo, T., Zhang, S., Dickman, D. K., & Anderson, D. J. (2019). Imaging neuropeptide release at synapses with a genetically engineered reporter. *ELife*, *8*. https://doi.org/10.7554/elife.46421

Doudna, J. A., & Charpentier, E. (2014). The new frontier of genome engineering with CRISPR-Cas9. *Science*. American Association for the Advancement of Science.

https://doi.org/10.1126/science.1258096

Dube, M. G., Sahu, A., Kalra, P. S., & Kalra, S. P. (1992). Neuropeptide Y release is elevated from the microdissected paraventricular nucleus of food-deprived rats: an in vitro study. *Endocrinology*, *131*(2), 684–688. https://doi.org/10.1210/endo.131.2.1639015

El Meskini, R., Jin, L., Marx, R., Bruzzaniti, A., Lee, J., Emeson, R. B., & Mains, R. E. (2001). A signal sequence is sufficient for green fluorescent protein to be routed to regulated secretory granules. *Endocrinology*, *142*(2), 864–873. https://doi.org/10.1210/endo.142.2.7929

Gamber, K. M., Macarthur, H., & Westfall, T. C. (2005). Cannabinoids augment the release of neuropeptide Y in the rat hypothalamus. *Neuropharmacology*, *49*(5), 646–652. https://doi.org/10.1016/j.neuropharm.2005.04.017

Gandasi, N. R., Vestö, K., Helou, M., Yin, P., Saras, J., & Barg, S. (2015). *Survey of Red Fluorescence Proteins as Markers for Secretory Granule Exocytosis*. https://doi.org/10.1371/journal.pone.0127801

Hall, J. E. (2019). Neuroendocrine Control of the Menstrual Cycle. *Yen & Jaffe's Reproductive Endocrinology: Physiology, Pathophysiology, and Clinical Management: Eighth Edition*. Elsevier Inc. https://doi.org/10.1016/B978-0-323-47912-7.00007-X

Han, Y., & Ding, K. (2022). Imaging Neuropeptide Release at *Drosophila* Neuromuscular Junction with a Genetically Engineered Neuropeptide Release Reporter. *Methods in Molecular Biology*, *2417*, 193–203. https://doi.org/10.1007/978-1-0716-1916-2_15

Heilig, M. (2004). The NPY system in stress, anxiety and depression. *Neuropeptides*. https://doi.org/10.1016/j.npep.2004.05.002

Hirsch, D., & Zukowska, Z. (2012). NPY and stress 30 years later: The peripheral view. *Cellular and Molecular Neurobiology*. https://doi.org/10.1007/s10571-011-9793-z

Hökfelt, T., Bartfai, T., & Bloom, F. (2003). Neuropeptides: Opportunities for drug discovery. *Lancet Neurology*. https://doi.org/10.1016/S1474-4422(03)00482-4

Hökfelt, T., Stanic, D., Sanford, S. D., Gatlin, J. C., Nilsson, I., Paratcha, G., Ledda, F., Fetissov, S., Lindfors, C., Herzog, H., Johansen, J. E., Ubink, R., & Pfenninger, K. H. (2008). NPY and its involvement in axon guidance, neurogenesis, and feeding. *Nutrition*. https://doi.org/10.1016/j.nut.2008.06.010

Hoyle, C. H. V. (1998). Neuropeptide families: Evolutionary perspectives. *Regulatory Peptides*. https://doi.org/10.1016/S0167-0115(97)01073-2

Hsu, P. D., Lander, E. S., & Zhang, F. (2014). Development and applications of CRISPR-Cas9 for genome engineering. *Cell*. https://doi.org/10.1016/j.cell.2014.05.010

Huttner, W. B., Gerdes, H. H., & Rosa, P. (1991). The granin-(chromogranin/secretogranin) family. *Trends in Biochemical Sciences*, *16*(C), 27–30. https://doi.org/10.1016/0968-0004(91)90012-K

Liu, A., Huang, X., He, W., Xue, F., Yang, Y., Liu, J., Chen, L., Yuan, L., & Xu, P. (2021). pHmScarlet is a pH-sensitive red fluorescent protein to monitor exocytosis docking and fusion steps. *Nature Communications*, *12*(1), 1–12. https://doi.org/10.1038/s41467-021-21666-7

Loh, K., Herzog, H., & Shi, Y. C. (2015). Regulation of energy homeostasis by the NPY system.

*Trends in Endocrinology and Metabolism*. https://doi.org/10.1016/j.tem.2015.01.003

Luquet, S., Perez, F. A., Hnasko, T. S., & Palmiter, R. D. (2005). NPY/AgRP neurons are essentials for feeding in adult mice but can be ablated in neonates. *Science*, *310*(5748), 683–685. https://doi.org/10.1126/science.1115524

Makhmutova, M., Liang, T., Gaisano, H., Caicedo, A., & Almaça, J. (2017). Confocal imaging of neuropeptide Y-pHluorin: A technique to visualize insulin granule exocytosis in intact murine and human islets. *Journal of Visualized Experiments*, *2017*(127). https://doi.org/10.3791/56089

Miesenböck, G., De Angelis, D. A., & Rothman, J. E. (1998). Visualizing secretion and synaptic transmission with pH-sensitive green fluorescent proteins. *Nature*, *394*(6689), 192–195. https://doi.org/10.1038/28190

Montero-Hadjadje, M., Vaingankar, S., Elias, S., Tostivint, H., Mahata, S. K., & Anouar, Y. (2007). Chromogranins A and B and secretogranin II: evolutionary and functional aspects. *Acta Physiologica*, *192*(2), 309–324. https://doi.org/10.1111/j.1748-1716.2007.01806.x

Nusbaum, M. P., Blitz, D. M., & Marder, E. (2017). Functional consequences of neuropeptide and small-molecule co-transmission. *Nature Reviews Neuroscience*. https://doi.org/10.1038/nrn.2017.56

Ou, X. M., Partoens, P. M., Wang, J. M., Walker, J. H., Danks, K., Vaughan, P. F., & De Potter, W. P. (1998). The storage of noradrenaline, neuropeptide Y and chromogranins in and stoichiometric release from large dense cored vesicles of the undifferentiated human neuroblastoma cell line SH-SY5Y. *International Journal of Molecular Medicine*, *1*(1), 105–112. https://doi.org/10.3892/ijmm.1.1.105

Parker, J. A., & Bloom, S. R. (2012). Hypothalamic neuropeptides and the regulation of appetite. *Neuropharmacology*. https://doi.org/10.1016/j.neuropharm.2012.02.004

Piedimonte, G. (1995). Tachykinin peptides, receptors, and peptidases in airway disease. *Experimental Lung Research*. Ihttps://doi.org/10.3109/01902149509031765

Podvin, S., Bundey, R., Toneff, T., Ziegler, M., & Hook, V. (2015). Profiles of secreted neuropeptides and catecholamines illustrate similarities and differences in response to stimulation by distinct secretagogues. *Molecular and Cellular Neuroscience*, *68*, 177–185. https://doi.org/10.1016/j.mcn.2015.06.008

Russo, A. F. (2017). Overview of Neuropeptides: Awakening the Senses? *Headache*, *57*(Suppl 2), 37–46. https://doi.org/10.1111/head.13084

Rutter, G. A., Loder, M. K., & Ravier, M. A. (2006). Rapid three-dimensional imaging of individual insulin release events by Nipkow disc confocal microscopy. *Biochemical Society Transactions*, *34*(5), 675–678. https://doi.org/10.1042/BST0340675

Setten, R. L., Rossi, J. J., & Han, S. ping. (2019). The current state and future directions of RNAi-based therapeutics. *Nature Reviews Drug Discovery*. https://doi.org/10.1038/s41573-019-0017-4

Svoboda, P. (2020). Key Mechanistic Principles and Considerations Concerning RNA Interference. *Frontiers in Plant Science*. https://doi.org/10.3389/fpls.2020.01237

Taupenot, L., Harper, K. L., & O'Connor, D. T. (2003). The Chromogranin–Secretogranin Family.

*New England Journal of Medicine*, *348*(12), 1134–1149. https://doi.org/10.1056/nejmra021405

van den Pol, A. N. (2012). Neuropeptide Transmission in Brain Circuits. *Neuron*. https://doi.org/10.1016/j.neuron.2012.09.014

Varadi, A., Tsuboi, T., & Rutter, G. A. (2005). Myosin Va transports dense core secretory vesicles in pancreatic MIN6 β-cells. *Molecular Biology of the Cell*, *16*(6), 2670–2680. https://doi.org/10.1091/mbc.E04-11-1001

Wang, X., Hu, R., Liang, J., Li, Z., Sun, W., & Pan, X. (2016). 5-HT7 Receptors Are Not Involved in Neuropeptide Release in Primary Cultured Rat Trigeminal Ganglion Neurons. *Journal of Molecular Neuroscience*, *59*(2), 251–259. https://doi.org/10.1007/s12031-016-0727-6

Williams, D. M., Nawaz, A., & Evans, M. (2020). Drug Therapy in Obesity: A Review of Current and Emerging Treatments. *Diabetes Therapy*. https://doi.org/10.1007/s13300-020-00816-y

Wilson, R. C., & Doudna, J. A. (2013). Molecular Mechanisms of RNA Interference. *Annual Review of Biophysics*, *42*(1), 217–239. https://doi.org/10.1146/annurev-biophys-083012-130404

Winkler, H., & Fischer-Colbrie, R. (1992). The chromogranins A and B: The first 25 years and future perspectives. *Neuroscience*, *49*(3), 497–528. https://doi.org/10.1016/0306-4522(92)90222-N

Yulyaningsih, E., Zhang, L., Herzog, H., & Sainsbury, A. (2011). NPY receptors as potential targets for anti-obesity drug development. *British Journal of Pharmacology*, *163*(6), 1170–1202. https://doi.org/10.1111/j.1476-5381.2011.01363.x

Zelikowsky, M., Hui, M., Gradinaru, V., Deverman, B. E., Anderson, D. J., Karigo, T., Choe, A., Yang, B., Blanco, M. R., Beadle, K., Gradinaru, V., Deverman, B. E., & Anderson, D. J. (2018). The Neuropeptide Tac2 Controls a Distributed Brain State Induced by Chronic Social Isolation Stress. *Cell*, *173*(5), 1265-1279.e19. https://doi.org/10.1016/j.cell.2018.03.037

Zhao, Y., Araki, S., Wu, J., Teramoto, T., Chang, Y. F., Nakano, M., Abdelfattah, A. S., Fujiwara, M., Ishihara, T., Nagai, T., & Campbell, R. E. (2011). An expanded palette of genetically encoded Ca2+ indicators. *Science*, *333*(6051), 1888–1891. https://doi.org/10.1126/science.1208592